ORIGINAL RESEARCH

Critical role of angiographic acquisition modality and reconstruction on morphometric and haemodynamic analysis of intracranial aneurysms

Alexandra Lauric, James E Hippelheuser, Adel M Malek

Cerebrovascular and Endovascular Division, Department of Neurosurgery, Tufts Medical Center, Tufts University School of Medicine, Boston, Massachusetts, USA

Correspondence to
Dr Adel M Malek, Department of Neurosurgery, Tufts Medical Center, Boston, MA 02111, USA; amalek@tuftsmedicalcenter.org

Received 6 December 2017
Accepted 21 December 2017
Published Online First 19 January 2018

ABSTRACT

Background Subtracted 3-D rotational angiography (3DRA) and cone-beam computed tomography angiography (CBCT-A) are often used in assessing cerebral aneurysm shape and haemodynamic profile. We sought to evaluate the effect of imaging modality, reconstruction parameters, and kernel selection on patient-derived aneurysm morphology and computational fluid dynamic (CFD) analysis to assess its potential contribution to inter-study variability.

Methods Four patients (five aneurysms) underwent concurrent 3DRA followed by high-resolution CBCT-A. Six models were reconstructed per aneurysm: 3DRA reconstructed with 0.28 and 0.14 mm voxel sizes (large and small volume of interest (VOI) respectively), and two kernel types (normal/smooth). CBCT-A was reconstructed over small VOI using normal/sharp kernel. Maximal dome dimension, neck diameter and dome/neck ratio were evaluated in 3D. Wall shear stress (WSS) magnitude was evaluated on the entire aneurysm dome and in the 5% dome areas covered by lowest (LWSS) and highest (HWSS) WSS. Parameters were evaluated with pairwise t-test analysis.

Results Smaller VOI reconstructions resulted in smaller D_{max} (P value=0.03) and D_{max}/neck (P value=0.006) and in larger LWSS (P value=0.03). Use of sharp kernel led to narrower neck (P value=0.04) and higher D_{max}/neck values (P value=0.02). CBCT-A resulted in statistically different aneurysm shape (up to 24% difference) and haemodynamics (up to 97% difference) compared with 3DRA.

Conclusion The choice of catheter 3D angiographic modality and reconstruction kernel has a critical impact on derived aneurysm morphological and haemodynamic analysis. The resultant variability can confound and obscure underlying differences within patient populations and between studies performed at different centres using divergent techniques, compromising the accuracy of quantitative aneurysm analysis.

INTRODUCTION

Despite having a relatively low risk of rupture, intracranial aneurysms account for the vast majority of non-traumatic subarachnoid haemorrhage, which is still associated with high mortality and morbidity.[1] Morphological and haemodynamic features of intracranial aneurysms are routinely evaluated for rupture risk stratification, treatment planning and care management. 3D rotational angiography (3DRA) is considered one of the most accurate acquisition technologies for aneurysm research, although studies also report on angiographic volumes imaged with lower spatial resolution, such as magnetic resonance (MRA) or computed tomography angiography (CTA).[1] In addition, studies often report results on mixed aneurysm databases from multiple acquisition modalities.[2–4] Recent studies have demonstrated the utility of cone beam computed tomography angiography (CBCT-A) with its spatial resolution being higher than 3DRA as a potentially more accurate alternative to 3DRA.[5]

Imaging modality has an impact on morphological analysis with differences between 3DRA, MRA,[6] CTA[7 8] and digital subtraction angiography (DSA).[9] Morphological differences were reported within the same CTA acquisition depending on reconstruction kernels.[7] Recent studies also suggested that acquisition modality could have an effect on the accuracy of aneurysm computational fluid dynamic (CFD) analysis.[8–10]

Given the prevalent use of 3D patient-derived models for intracranial aneurysm analysis, and multicentre datasets from multiple acquisition modalities and reconstruction types, we aim here to assess morphological and heamodynamic variability and reproducibility in aneurysm shape and CFD evaluation. Using the highest available catheter-based rotational angiography we would expect relatively little variation; however, the extent of such differences is unknown. Accordingly, we hypothesised that differences detected during clinical use of the 3D imaging workflow in intracranial aneurysm treatment may lead to significant differences in results. We thus evaluate changes in morphometric and computational haemodynamic analysis of a series of aneurysms as a result of different catheter-based image modalities (3DRA and CBCT-A), different reconstruction kernels, and image resolutions.

MATERIALS AND METHODS

Patient selection and demographics

Five aneurysms (in four random patients) were selected from consecutive patients presenting with intracranial aneurysm, who had undergone the angiography under general anaesthesia to ensure absence of motion artifact (figure 1A). Fusiform, mycotic and extradural aneurysms were excluded. Locations included internal carotid artery (aneurysm 1), anterior communicating artery aneurysm (aneurysm 2), middle cerebral artery aneurysm

Check for updates

To cite: Lauric A, Hippelheuser JE, Malek AM. *J NeuroIntervent Surg* 2018;**10**:911–915.

J NeuroIntervent Surg: first published as 10.1136/neurintsurg-2017-013677 on 19 January 2018. Downloaded from http://jnis.bmj.com/ on November 15, 2026 at Tufts University Libraries. Protected by copyright, including for uses related to text and data mining, AI training, and similar technologies.

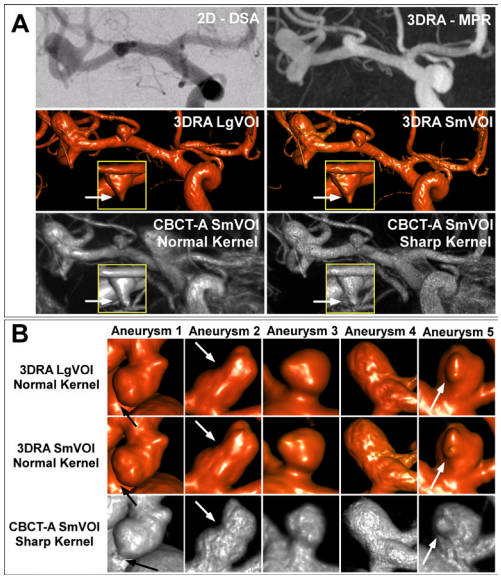


Figure 1 (A) Imaging reconstruction for aneurysms 4 and 5. Aneurysm 4 is located at the middle cerebral artery bifurcation. Aneurysm 5 is located at the origin of the anterior temporal artery. 2D-DSA (2D digital subtraction angiography), 3DRA-MPR (3D rotational angiography, multiplanar reconstruction), 3DRA LgVOI (3DRA reconstructed over a large volume of interest), 3DRA SmVOI (3DRA reconstructed over a small volume of interest), CBTA-A SmVOI normal kernel (cone beam CT angiography reconstructed over small VOI with normal kernel), CBTA-A SmVOI sharp kernel (cone-beam CT angiography reconstructed over small VOI with sharp kernel). The arrows point to differences in aneurysm features between 3DRA and CBCT-A. In aneurysm 5, CBCTA-A shows a clearly defined focal bleb (arrow) that is less well defined on 3DRA acquisitions. (B) 3D volume visualisation for 3DRA and CBCT-A, for the entire aneurysm dataset. The arrows point to differences in aneurysm features between 3DRA and CBCT-A. In aneurysm 1, CBCT-A reveals a bleb not detected on 3DRA (arrow); in aneurysm 2, smaller VOI and CBCT-A delineate a waist between the main aneurysm and the superior daughter (arrow). In aneurysm 5, CBCTA-A shows a clearly defined focal bleb (arrow) that is less well defined on 3DRA acquisitions.

(aneurysm 3), right middle cerebral artery aneurysm, and right anterior temporal artery origin aneurysm (aneurysms 4 and 5, respectively). All angiographic imaging was obtained in an urgent fashion and prior to treatment or vasospasm onset.

Cerebral angiography and data processing

Three-dimensional catheter-based cerebral angiograms were all obtained under general anaesthesia and respiration was held during the acquisition run to minimise any motion artifact from lung inflation. All patients underwent cerebral angiography on a calibrated flat-panel biplanar DSA system (Artis, Siemens, Malvern, PA, USA). Conventional DSA was performed of the internal carotid artery (figure 1), which was followed in sequence by 3DRA (5 s acquisition, three cc/s contrast injection with 1 s pre-inject) and CBCT-A (20 s acquisition, one cc/s contrast injection with 2 s pre-inject) immediately thereafter. Vertebral artery acquisitions were not used to avoid contrast mixing from the contralateral vessel at the vertebrobasilar junction that could confound results.[11] Parameters for the 20 s CBCT-A acquisition were kVP=70 kV, mas=1.2 μGy/pulse, and focal point=0.6 mm. No mask run was performed prior to acquisition.

Acquisitions were reconstructed using the Leonardo software package (Siemens) to yield three-dimensional volumetric datasets, including the aneurysm and parent vessels. 3DRA volumes were reconstructed using subtraction Hounsfield units (HU) and preset volume of interest (VOI) with resolutions of 0.28 mm (large VOI, LgVOI) and 0.14 mm (small VOI, SmVOI) isotropic voxel size. In addition, the 3DRA volumes were reconstructed using normal, smooth and sharp kernel characteristics. The sharp 3DRA reconstructed volumes, however, were of insufficient quality for accurate segmentation because of high-frequency noise content, and were not included in this study. Consequently, for each patient, four reconstructed 3DRA volumes were available: (1) LgVOI normal kernel, (2) SmVOI normal kernel, (3) LgVOI smooth kernel, and (4) SmVOI smooth kernel. CBCT-A was reconstructed at SmVOI only, using both normal and sharp kernel characteristics. This resulted in two reconstructed volumes: (1) SmVOI normal kernel and (2) SmVOI sharp kernel.

All volumetric datasets were analysed in Amira version 5.3 (Thermo Fisher Scientific, Hillsboro, OR) for segmentation in 3D space. For each patient, the 3DRA LgVOI, normal kernel, was considered the reference model and was segmented as previously described using 3D gradient edge-detection filtering.[12] All other models (3DRA and CBCT-A) were segmented in Amira, such that the diameter of the parent vessel leading to the aneurysm was the same size as in the reference model.

Morphological feature extraction

Aneurysm morphology was evaluated in 3D space in Amira 5.3. The aneurysm neck was determined using a cross-sectional plane and the neck area and average diameter were automatically computed. The aneurysm dome was separated from the parent vessel using the neck plane, and the maximal dome size (D_{max}) was automatically evaluated as the maximal distance between any two points on the dome.[13] The dome/neck ratio was reported as the ratio between D_{max} and the average neck diameter.[13]

Computational fluid dynamics

The segmented surfaces were used to create polyhedral meshes of approximately 1 000 000 cells with a boundary layer enhancement using Star-CCM+ (CD-Adapco, Melville, New York, USA). The segment proximal to the site of the aneurysm was kept sufficiently long (at least five times the diameter of the parent vessel) in order to enable laminar flow to become fully developed and avoid entrance effects. CFD simulation was performed using Star-CCM+ (CD-Adapco), by modelling steady-state flow using 0.1 m/s constant inlet velocity, and zero outlet gauge pressure.[14]

Post-processing analysis was performed using EnSight 10.0 (Computational Engineering International, Apex, NC). WSS was evaluated as spatial mean on the aneurysm dome (TAWSS), as well as average on the 5% dome area covered by the lowest (LWSS) and highest (HWSS) WSS, as previously reported.[15]

Statistical analysis

JMP statistical software (version 13.0.0, SAS Institute, Cary, North Carolina, USA) was used to evaluate differences between the six reconstructions groups. Statistical significance was assumed for $P<0.05$. All variables were tested independently using the pairwise t-test analysis. Matched pair analysis ensures that each aneurysm acts as its own control.

RESULTS

Shape analysis

Large differences were noted both qualitatively (by observing the shape of the aneurysms) and quantitatively (morphological analysis) between different reconstruction models (figure 1B).

J NeuroIntervent Surg: first published as 10.1136/neurintsurg-2017-013677 on 19 January 2018. Downloaded from http://jnis.bmj.com/ on November 15, 2026 at Tufts University Libraries. Protected by copyright, including for uses related to text and data mining, AI training, and similar technologies.

Table 1 Matched pair statistical analysis of morphological and haemodynamic parameters using small and large volume of interest (SmVOI and LgVOI) reconstruction

	3DRA LgVOI Normal kernel	3DRA SmVOI Normal kernel	P value
D_{max}(mm)	5.06±1.62	5.19±1.63	0.03
Neck (mm)	3.31±0.97	3.31±0.99	0.81
D_{max}/neck	1.52±0.16	1.56±0.15	0.006
TAWSS (Pa)	0.24±0.12	0.22±0.11	0.33
LWSS (Pa)	0.008±0.007	0.006±0.006	0.03
HWSS (Pa)	1.51±0.86	1.53±0.86	0.88
	3DRA SmVOI Normal kernel	**CBCT-A SmVOI Sharp kernel**	**P value**
D_{max}(mm)	5.19±1.63	5.28±1.77	0.43
Neck (mm)	3.31±0.99	3.07±1.12	0.04
D_{max}/neck	1.56±0.15	1.73±0.15	0.02
TAWSS (Pa)	0.22±0.11	0.22±0.15	0.86
LWSS (Pa)	0.006±0.006	0.008±0.02	0.55
HWSS (Pa)	1.53±0.86	1.35±0.76	0.42
	3DRA LgVOI Smooth kernel	**CBCT-A SmVOI Sharp kernel**	**P value**
D_{max}(mm)	4.88±1.81	5.28±1.77	0.06
Neck (mm)	3.35±1.05	3.07±1.12	0.07
D_{max}/neck	1.44±0.22	1.73±0.15	0.02
TAWSS (Pa)	0.26±0.17	0.22±0.15	0.35
LWSS (Pa)	0.02±0.02	0.008±0.02	0.05
HWSS (Pa)	1.67±1.05	1.35±0.76	0.2

D_{max} is the maximal dimension of the aneurysm. Neck size is the averaged diameter of the neck plane. Time-averaged wall shear stress (TAWSS) was evaluated as dome averaged and on the 5% dome area covered by lowest (LWSS) and highest (HWSS) wall shear stress. Statistical significance was assumed for P<0.05.
3DRA, 3D rotational angiography; CBCT-A, cone beam CT angiography.

Use of SmVOI resulted in significantly higher D_{max} (P value=0.03) and D_{max}/neck (P value=0.006) (table 1). In addition, use of CBCT-A and sharp kernel resulted in significantly smaller neck values (P value=0.04) compared with 3DRA normal kernel. For all aneurysms, CBCT-A models resulted in higher D_{max}/neck ratio compared with 3DRA. Both the size of the neck and the D_{max}/neck ratio have potential clinical implications when choosing the most appropriate treatment strategy[16] and were previously shown to have rupture status discrimination.[17]

Morphological differences were particularly evident for smaller aneurysms, such as aneurysms 3 and 5. For instance, the size of aneurysm 5 varied between 3.97 mm (3DRA smooth kernel) and 5.05 (CBCT-A sharp kernel), a 27% difference (table 2). Similarly D_{max}/neck ratio varied between 1.15 (3DRA smooth kernel) and 1.68 (CBCT-A sharp kernel), a 46% difference (table 2).

In addition to differences in the size of aneurysmal models, the choice of reconstruction and modality had an impact on the shape of the aneurysms. In our dataset, this was particularly evident in the case of aneurysms 2 and 5. For aneurysm 2, 3DRA data show an elongated aneurysm with small blebs, whereas CBCT-A imaging suggests an initial aneurysm with a daughter aneurysm (figure 1B). Aneurysm 5 features a prominent bleb, which is less defined in 3DRA data, but clearly visible in CBCT-A volume (figure 1B).

Computational fluid dynamics

While the average dome TAWSS was relatively stable across different reconstructions, use of small VOI resulted in significantly lower LWSS (P value=0.03). This is the average WSS in the 5% area covered by lowest WSS.[15] This low WSS, but not TAWSS was previously associated with rupture status in aneurysms.[14 15] In addition, use of CBCT-A and sharp kernel resulted similarly in significantly lower LWSS (P value=0.05) compared with 3DRA smooth kernel.

Figure 2 shows the WSS distribution on the aneurysm's surface. While the main characteristics of the flow (as depicted by velocity profiles and streamlines) are maintained between modality/reconstruction models, there are subtle but important differences. It is evident from the TAWSS histograms (figure 2B) that the WSS distribution varies between models, with dramatic impact on the lower WSS range which has been proposed as predictive in rupture status classification.[14] This was true for all aneurysms evaluated in this study.

One of the patients included in the study harboured two aneurysms (number 4 and 5). Both aneurysms originated off the right middle cerebral artery, aneurysm 4 at the middle cerebral artery bifurcation, and aneurysm 5 at the origin of the anterior temporal artery (figure 1). Despite sharing an identical haemodynamic environment, aneurysm 5 (figure 2B) was more sensitive to the choice of image resolution, kernel and modality compared with aneurysm 4 (figure 2A), especially in the areas of low WSS (table 2). The well defined bleb on the surface of aneurysm 5, clearly defined in CBCT-A reconstructions, but not evident in 3DRA images, has very low WSS, which accounts for the dramatic two-order of magnitude LWSS

Table 2 Morphological and haemodynamic parameters for aneurysm 5 (right anterior temporal artery origin aneurysm)

	3DRA LgVOI Normal kernel (%)	3DRA LgVOI Smooth kernel (%)	3DRA SmVOI Normal kernel (%)	3DRA SmVOI Smooth kernel (%)	CBCT-A SmVOI Normal kernel (%)	CBCT-A SmVOI Sharp kernel (%)
D_{max}(mm)	4.47 (0)	4.05 (+9)	4.67 (–4.5)	3.97 (+11.2)	5.02 (–12.3)	5.05 (+13)
Neck size (mm)	3.3 (0)	3.47 (–5)	3.33 (–1)	3.46 (–5)	3.11 (+6)	3 (+9)
D_{max}/neck	1.35 (0)	1.17 (+13)	1.41 (–4)	1.15 (+15)	1.62 (–20)	1.68 (–24)
TAWSS (Pa)	0.091 (0)	0.128 (–41)	0.077 (+15)	0.126 (–38)	0.066 (+27)	0.045 (+50)
LWSS [Pa	0.003 (0)	0.014 (–327)	0.002 (+48)	0.011 (–245)	0.0001 (+97)	0.0001 (+97)
HWSS (Pa)	0.538 (0)	0.713 (–33)	0.438 (+19)	0.704 (–31)	0.527 (+2)	0.359 (+33)

Shown are actual values and corresponding percentage difference. D_{max} is the maximal dimension of the aneurysm. Neck size is the averaged diameter of the neck plane. Data volumes were reconstructed over small and large volume of interests (SmVOI and LgVOI). Time averaged wall shear stress (WSS) was evaluated as dome averaged and on the 5% dome area covered by lowest (LWSS) and highest (HWSS) wall shear stress. For % difference computation 3D rotational angiography (3DRA) LgVOI normal kernel is considered as reference. The % difference between variable V1 versus variable V2 is computed as 100*(V1–V2)/V1. CBCT-A, cone beam CT angiography,

J NeuroIntervent Surg: first published as 10.1136/neurintsurg-2017-013677 on 19 January 2018. Downloaded from http://jnis.bmj.com/ on November 15, 2026 at Tufts University Libraries . Protected by copyright, including for uses related to text and data mining, AI training, and similar technologies.

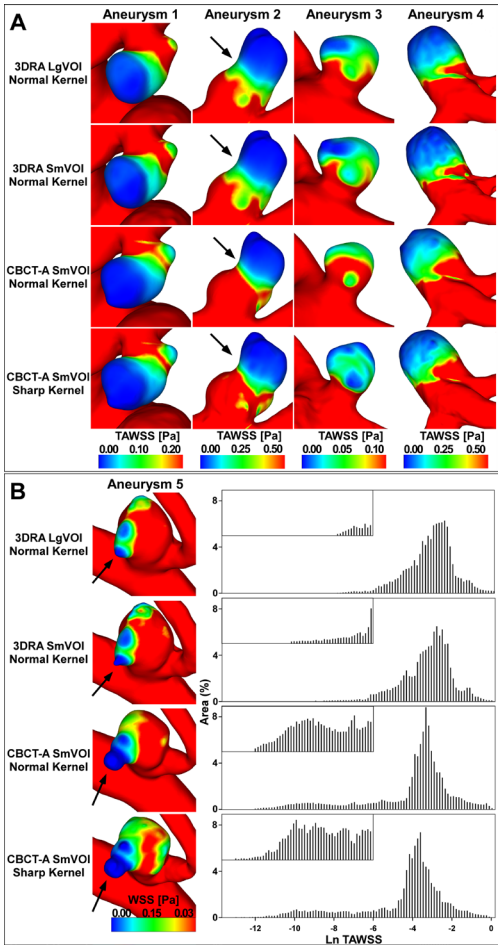


Figure 2 (A) Computational fluid dynamic simulations for aneurysms 1, 2, 3 and 4. Details are shown for 3D rotational angiography (3DRA) and cone beam CT angiography (CBCT-A) reconstructions. The arrows point to aneurysm features not visible in 3DRA volumes, but revealed by CBCT-A. (B) Time-averaged wall shear stress (TAWSS) on the dome of aneurysm 5, with the corresponding histograms for 3DRA and CBCT-A reconstruction models. Shape differences are clearly visible between 3DRA and CBCT-A segmentations, resulting in large variations of the low TAWSS range. The arrows point to aneurysm features not visible in 3DRA volumes, but revealed by CBCT-A. Lg VOI, large volume of interest; SmVOI, small volume of interest; WSS, wall shear stress.

differences (range 0.01–0.0001 Pa) between the two modalities (table 2).

DISCUSSION

Morphological and CFD analyses are increasingly used for clinical evaluation, rupture risk stratification, and treatment planning of intracranial aneurysms.[18–21] Aneurysm research is being reported on growing aneurysm datasets, from multiple acquisition and reconstruction types, sometimes combined.[2–4] While most research is concerned with identifying and validating reliable parameters for aneurysm analysis,[13 14 22] little is known about the effect of imaging heterogeneity on aneurysm evaluation. Emerging evidence suggests that the choice of reconstruction and acquisition imaging can have a significant effect on quantitative analysis and can introduce preprocessing bias.[7–10] Geers *et al*[8] reported that CTA models tend to have larger aneurysm necks, as well as larger dome WSS (up to 80% difference), compared with 3DRA-derived models. Lauric *et al*[10] reported dramatic differences in the shape of a ruptured anterior communicating artery aneurysm imaged with both 3DRA and CBCT-A; CBCT-A provided greater details, revealing the presence of a discrete irregular and elongated bleb, the likely rupture site, which was not visible on 3DRA. O'Meara *et al*[7] evaluated the impact of the CTA reconstruction kernel on pretreatment planning of ruptured intracranial aneurysms; despite resulting in a less visually pleasing image, the sharp kernel provided a more accurate estimation of the neck size and the vessels near the neck of the aneurysm, which in turn allowed for more accurate pretreatment assessment.

This study shows that small VOI reconstructions resulted in larger aneurysm sizes and narrower necks, as did choice of sharp compared with smooth/normal kernels. 3DRA models had smaller aneurysm sizes and larger neck diameters compared with the corresponding CBCT-A models, which resulted in higher CBCT-A dome/neck ratio for all aneurysms. Accurate estimation of dome/neck ratio is essential for treatment planning,[16] as higher dome/neck ratio is a favourable parameter for coil occlusion, and can be critical for the determination of whether an aneurysm should be treated by an endovascular versus microsurgical approach.[16]

Whereas previous studies on aneurysm phantoms suggested that aneurysm morphology is robust to modality,[6 23] we show that small and irregularly shaped aneurysms are sensitive to choice of modality. CBCT-A imaging can reveal aneurysm features not visible on 3DRA imaging, as is the case with aneurysm 5. Here CBCT-A reveals a prominent bleb on the aneurysm surface, an important finding given that bleb presence is considered a risk factor for aneurysmal rupture.[24] In the case of aneurysm 2, THE CBCT-A-derived model suggested a bilobed aneurysm (potential risk factor for aneurysmal rupture), quite distinct from the elongated 3DRA-derived aneurysm morphology. It is likely that, beyond the higher sensitivity of CBCT-A, the longer acquisition time (20 s for CBCT-A vs 5 s for 3DRA) allows for contrast to diffuse into the entire aneurysm dome, resulting in a better separation from the nearby structures and increased detail of the aneurysm structure. The longer temporal acquisition of CBCT-A (20 s vs 5 s) may enable better capture of the aneurysm properties that could be blurred during a shorter sampling period, such as beat-to-beat pulsation of the aneurysm. Future research is needed to evaluate the effect of such beat-to-beat cardiac-induced motion.

Intracranial aneurysm imaging for CFD analysis is a complex process with each step potentially influencing the analysis.[25 26] There have been numerous studies denouncing the utility of CFD and the potential for confounding results.[27 28] This study suggests that in addition to all other sources of variability[11 26] (meshing resolution and technique,[29] CFD solver and parameters,[30 31] boundary conditions, etc.), a significant source of variability that can unsettle the robustness of aneurysm haemodynamics research is the initial reconstruction parameters even when obtained in the same patient and the same settings contemporaneously, using the highest available resolution imaging, in a patient who is immobilised during general anaesthesia and under apneic conditions. Here the aneurysms acted as their own controls; the same modality/reconstruction models were available for all aneurysms and the results were compared within each aneurysm simulation. In general, LWSS distribution seemed more sensitive to modality/reconstruction type compared with TAWSS and HWSS. This is particularly relevant for intracranial aneurysm research when assuming the low WSS hypothesis for aneurysm rupture risk.[14 22]

Interestingly, despite sharing an identical haemodynamic environment (within the same patient and on the same parent vessel),

J NeuroIntervent Surg: first published as 10.1136/neurintsurg-2017-013677 on 19 January 2018. Downloaded from http://jnis.bmj.com/ on November 15, 2026 at Tufts University Libraries. Protected by copyright, including for uses related to text and data mining, AI training, and similar technologies.

aneurysm 5 (figure 2B) was more sensitive to VOI size, kernel and modality variations compared with aneurysm 4 (figure 2A). Likely this is because of its smaller size and irregular shape. Whereas for aneurysm 4, CBCT-A resulted in higher TAWSS values compared with 3DRA, the opposite was true for aneurysm 5. This underlines the fact that no assumptions can be made regarding the aneurysm model behaviour across acquisition types.

Previous studies reported on the importance of ensuring standardised measuring protocols for morphometric aneurysm analysis.[13] Here we argue for increased awareness when reporting on mixed aneurysm datasets, and when attempting multiple study reviews. Even using the same acquisition technology from a particular manufacturer, the same equipment, and the same patient minutes apart, dramatically different results can be obtained depending on the acquisition technique (3DRA vs CBCT-A). Moreover, using the same acquisition technique, the choice of reconstruction parameters also affected the results significantly. Whereas such wide variability would have been expected among modalities such as MRA and CTA, it was surprising to see so much difference even when using higher accuracy catheter-based angiography.

Study limitations

While this study suggests that the choice of acquisition and reconstruction parameters may have clinical implications, the practical applicability of these observations has to be clarified under clinical conditions. The segmentation of 3DRA large VOI, normal kernel was used as guidance when creating the rest of the models to control for variations in parent vessel size, and isolate the effect of acquisition and reconstruction on aneurysm haemodynamics. As a result, the effect of segmentation on modality and reconstruction was not taken into account in this study. Moreover, this study was only concerned with 3DRA and CBCT-A imaging, and the only reconstruction variables considered were VOI size and kernel type.

CONCLUSION

Using different modality and reconstruction types for cerebral aneurysm analysis has considerable effects on both morphological and haemodynamic analyses, even within catheter-based rotational angiography. Small VOI, sharp kernels, and use of CBCT-A resulted in smaller dome/neck and lower WSS, a finding with potentially important clinical applications. CBCT-A might provide for a higher level of detail in the region of interest, possibly resulting in more accurate morphological and haemodynamic analysis. Importantly, this study highlights the risk of mixing models across imaging modalities and reconstructions when performing quantitative aneurysm analysis. These data suggest the need for consensus building and standard setting to enable more accurate and robust multicentre multinational analyses and minimise artefactual measurements that can obscure critical morphometric and haemodynamic features, which are needed to understand the underlying pathophysiology.

Contributors The research is original and each author provided significant contribution to the work.

Funding This work was supported by a fellowship support from Medtronic Inc. and Microvention Inc.

Competing interests The senior author (AMM) has received research funding from Stryker for research that is unrelated to the submitted work.

Patient consent Detail has been removed from this case description/these case descriptions to ensure anonymity. The editors and reviewers have seen the detailed information available and are satisfied that the information backs up the case the authors are making.

Ethics approval This research was approved by Tufts Health Sciences Campus Institutional Review Board.

Provenance and peer review Not commissioned; externally peer reviewed.

© Article author(s) (or their employer(s) unless otherwise stated in the text of the article) 2018. All rights reserved. No commercial use is permitted unless otherwise expressly granted.

REFERENCES

1 Lawton MT, Vates GE. Subarachnoid hemorrhage. *N Engl J Med* 2017;377:257–66.
2 Amenta PS, Yadla S, Campbell PG, *et al*. Analysis of nonmodifiable risk factors for intracranial aneurysm rupture in a large, retrospective cohort. *Neurosurgery* 2012;70:693–701.
3 Chien A, Sayre J, Viñuela F. Comparative morphological analysis of the geometry of ruptured and unruptured aneurysms. *Neurosurgery* 2011;69:349–56.
4 Xiang J, Natarajan SK, Tremmel M, *et al*. Hemodynamic-morphologic discriminants for intracranial aneurysm rupture. *Stroke* 2011;42:144–52.
5 Rahal JP, Malek AM. Benefit of cone-beam computed tomography angiography in acute management of angiographically undetectable ruptured arteriovenous malformations. *J Neurosurg* 2013;119:1015–20.
6 Goubergrits L, Schaller J, Kertzscher U, *et al*. Reproducibility of image-based analysis of cerebral aneurysm geometry and hemodynamics: an in-vitro study of magnetic resonance imaging, computed tomography, and three-dimensional rotational angiography. *J Neurol Surg A Cent Eur Neurosurg* 2013;74:294–302.
7 O'meara B, Rahal JP, Lauric A, *et al*. Benefit of a sharp computed tomography angiography reconstruction kernel for improved characterization of intracranial aneurysms. *Neurosurgery* 2014;10:97–105.
8 Geers AJ, Larrabide I, Radaelli AG, *et al*. Patient-specific computational hemodynamics of intracranial aneurysms from 3D rotational angiography and CT angiography: an in vivo reproducibility study. *AJNR Am J Neuroradiol* 2011;32:581–6.
9 Schneiders JJ, Marquering HA, Antiga L, *et al*. Intracranial aneurysm neck size overestimation with 3D rotational angiography: the impact on intra-aneurysmal hemodynamics simulated with computational fluid dynamics. *AJNR Am J Neuroradiol* 2013;34:121–8.
10 Lauric A, Heller RS, Schimansky S, *et al*. Benefit of cone-beam CT angiography in visualizing aneurysm shape and identification of exact rupture site. *J Neuroimaging* 2015;25:56–61.
11 Jou LD, Mohamed A, Lee DH, *et al*. 3D rotational digital subtraction angiography may underestimate intracranial aneurysms: findings from two basilar aneurysms. *AJNR Am J Neuroradiol* 2007;28:1690–2.
12 Baharoglu MI, Lauric A, Wu C, *et al*. Deviation from optimal vascular caliber control at middle cerebral artery bifurcations harboring aneurysms. *J Biomech* 2014;47:3318–24.
13 Lauric A, Baharoglu MI, Malek AM. Ruptured status discrimination performance of aspect ratio, height/width, and bottleneck factor is highly dependent on aneurysm sizing methodology. *Neurosurgery* 2012;71:38–46.
14 Lauric A, Hippelheuser J, Cohen AD, *et al*. Wall shear stress association with rupture status in volume matched sidewall aneurysms. *J Neurointerv Surg* 2014;6:466–73.
15 Hippelheuser JE, Lauric A, Cohen AD, *et al*. Realistic non-newtonian viscosity modelling highlights hemodynamic differences between intracranial aneurysms with and without surface blebs. *J Biomech* 2014;47:3695–703.
16 Brinjikji W, Cloft HJ, Kallmes DF. Difficult aneurysms for endovascular treatment: overwide or undertall? *AJNR Am J Neuroradiol* 2009;30:1513–7.
17 Baharoglu MI, Lauric A, Gao BL, *et al*. Identification of a dichotomy in morphological predictors of rupture status between sidewall- and bifurcation-type intracranial aneurysms. *J Neurosurg* 2012;116:871–81.
18 Kono K, Shintani A, Fujimoto T, *et al*. Stent-assisted coil embolization and computational fluid dynamics simulations of bilateral vertebral artery dissecting aneurysms presenting with subarachnoid hemorrhage: case report. *Neurosurgery* 2012;71:E1192–201.
19 Chung B, Cebral JR. CFD for evaluation and treatment planning of aneurysms: review of proposed clinical uses and their challenges. *Ann Biomed Eng* 2015;43:122–38.
20 Ventikos Y, Holland EC, Bowker TJ, *et al*. Computational modelling for cerebral aneurysms: risk evaluation and interventional planning. *Br J Radiol* 2009;82 Spec No 1:S62–71.
21 Lall RR, Eddleman CS, Bendok BR, *et al*. Unruptured intracranial aneurysms and the assessment of rupture risk based on anatomical and morphological factors: sifting through the sands of data. *Neurosurg Focus* 2009;26:E2.
22 Meng H, Tutino VM, Xiang J, *et al*. High WSS or low WSS? Complex interactions of hemodynamics with intracranial aneurysm initiation, growth, and rupture: toward a unifying hypothesis. *AJNR Am J Neuroradiol* 2014;35:1254–62.
23 Ramachandran M, Retarekar R, Harbaugh RE, *et al*. Sensitivity of quantified intracranial aneurysm geometry to imaging modality. *Cardiovasc Eng Technol* 2013;4:75–86.
24 Cebral JR, Sheridan M, Putman CM. Hemodynamics and bleb formation in intracranial aneurysms. *AJNR Am J Neuroradiol* 2010;31:304–10.
25 Spiegel M, Redel T, Zhang YJ, *et al*. Tetrahedral vs. polyhedral mesh size evaluation on flow velocity and wall shear stress for cerebral hemodynamic simulation. *Comput Methods Biomech Biomed Engin* 2011;14:9–22.

J NeuroIntervent Surg: first published as 10.1136/neurintsurg-2017-013677 on 19 January 2018. Downloaded from http://jnis.bmj.com/ on November 15, 2026 at Tufts University Libraries. Protected by copyright, including for uses related to text and data mining, AI training, and similar technologies.

26 Hernandez M, Frangi AF. Non-parametric geodesic active regions: method and evaluation for cerebral aneurysms segmentation in 3DRA and CTA. *Med Image Anal* 2007;11:224–41.
27 Xiang J, Tutino VM, Snyder KV, *et al*. CFD: computational fluid dynamics or confounding factor dissemination? The role of hemodynamics in intracranial aneurysm rupture risk assessment. *AJNR Am J Neuroradiol* 2014;35:1849–57.
28 Kallmes DF. Point: CFD--computational fluid dynamics or confounding factor dissemination. *AJNR Am J Neuroradiol* 2012;33:395–6.
29 Cebral JR, Castro MA, Appanaboyina S, *et al*. Efficient pipeline for image-based patient-specific analysis of cerebral aneurysm hemodynamics: technique and sensitivity. *IEEE Trans Med Imaging* 2005;24:457–67.
30 Valen-Sendstad K, Steinman DA. Mind the gap: impact of computational fluid dynamics solution strategy on prediction of intracranial aneurysm hemodynamics and rupture status indicators. *AJNR Am J Neuroradiol* 2014;35:536–43.
31 Dennis KD, Kallmes DF, Dragomir-Daescu D. Cerebral aneurysm blood flow simulations are sensitive to basic solver settings. *J Biomech* 2017;57:46–53.

J NeuroIntervent Surg: first published as 10.1136/neurintsurg-2017-013677 on 19 January 2018. Downloaded from http://jnis.bmj.com/ on November 15, 2026 at Tufts University Libraries .
Protected by copyright, including for uses related to text and data mining, AI training, and similar technologies.